Understanding melting due to ocean eddy heat fluxes at the edge of sea-ice floes

Christopher Horvat[1,2], **Eli Tziperman**[2]

[1]Institute at Brown for Environment and Society, Brown University, Providence, RI, 02912, USA.

[2]Department of Earth and Planetary Sciences and School of Engineering and Applied Sciences, Harvard University, Cambridge, MA, 02138, USA

XXX CHECK ALL FIGURES, LEGENDS, ETC FOR CORRECT COLORING. CHECK EVERY FIGURE REFERENCE. XXX

Key Points:

- Sub-mesoscale ocean eddies energized at static melting sea-ice floe edges lead to strong heat transport between open ocean and ice covered areas.
- Such eddies can significantly enhance the melting rate of sea ice, yet are not represented in current climate models.
- We outline a representation of these eddy heat fluxes that captures the melting of sea ice that can be used to improve future sea ice models.

Corresponding author: Christopher Horvat, horvat@brown.edu

Abstract

Understanding how upper-ocean heat content evolves and affects sea ice in the polar regions is necessary to predict past, present, and future weather and climate. The sea-ice cover, a composite of individual floes, varies significantly on scales as small as meters, and as a result the ocean buoyancy field may be inhomogeneous at scales unresolved in current climate models. Lateral gradients in surface heating at the edge of floes can energize sub-grid-scale ocean eddies that mix heat in the surface layer and control sea-ice melting. Here, the development of baroclinic instability near floe edges is investigated using a high-resolution ocean circulation model, representing a single grid cell of a climate model partially covered in thin, static sea ice. From the resulting ocean circulation we characterize and parameterize the strength of eddy-induced lateral mixing and heat transport, and the effects on sea-ice melting, as a function of state variables resolved in global climate models.

1 Introduction

Through its albedo and mediation of ocean-atmosphere heat exchange, Earth's sea-ice cover plays an important role in the climate system. Arctic sea ice volumes have declined rapidly in the satellite era, leading to a reduction in surface albedo that is the main cause of the rapid warming of the Arctic [*Screen and Simmonds*, 2010]. The loss of Arctic sea ice coincides with a transition from a thick, perennial Arctic sea-ice cover to a seasonal one: most of the current Arctic Ocean is covered in thin, first-year ice that grows in winter and melts entirely in summer [*Maslanik et al.*, 2011]. The growth of sea ice in winter is tightly coupled to the depth and heat content of the ice-covered ocean mixed layer, major uncertain factors in the polar climate system [*Peralta-Ferriz and Woodgate*, 2015]. Nearly half of the melting of summer Arctic sea ice occurs at its base, i.e. due to heat fluxes from the ocean to the ice [*Perovich*, 2003; *Lei et al.*, 2014; *Perovich et al.*, 2014]. In turn, the seasonal cycle of ocean heat content is coupled to the seasonal evolution of sea ice, which mediates the heating and mixing of the polar oceans. This tight coupling between sea ice and upper ocean variability has resulted in a lengthening of the Arctic sea-ice melt season over the satellite era as the Arctic Ocean has warmed and Arctic sea ice has retreated [*Markus et al.*, 2009].

Sea ice is a composite of individual floes, each identified with a horizontal scale, or "size". Floe sizes span a wide range, and play a critical role in floes' thermodynamic evo-

lution. For floes smaller than 100 meters, lateral (along the floe edge) melting is a dominant component of thermodynamic evolution of sea ice [*Steele*, 1992; *Horvat and Tziperman*, 2015]. Yet ocean eddies with scales of several kilometers or smaller may be energized in regions where gradients in sea ice concentration lead to gradients in upper-ocean properties, such as within the marginal ice zone [e.g., *Hakkinen*, 1986; *Manucharyan and Thompson*, 2017], or at an ice edge *Matsumura and Hasumi* [2008]; *Årthun et al.* [2013]. If such eddies are energized by the melting of a floe they may potentially determine its melt rate as a function of its size [*Horvat et al.*, 2016].

While there have been limited and indirect observations of the impact of kilometer scale ocean variability at floe edges in summer [for example, *Perovich*, 2003], eddies generated at floe boundaries during the melt season have the potential to mix ocean heat laterally from the warmer open water to under the ice. This eddy heat transport can melt sea ice at its base near floe edges, leading to a strong dependence of the melting rate of sea ice on floe size. Current ocean/sea-ice models assume that any heating applied to open water by the atmosphere is instantaneously mixed throughout the grid cell, though in reality there is a partitioning of heat content between open water regions and under-ice regions [*Holland*, 2003]. It is therefore important to constrain and understand the strength of upper-ocean lateral mixing process, as current sea ice models are coarse continuum models, and are not capable of resolving ocean mixing across the floe edge.

Past work has focused on the mechanical interactions between sea ice and the existing upper ocean density structure in the marginal ice zone (i.e., *Manucharyan and Thompson* [2017]). Here we instead focus on the development of baroclinic instability near a single static ice boundary during the melt season, extending the study of *Horvat et al.* [2016] and moving towards a parameterization of the effect of ocean eddies for climate modeling purposes. Examining this purely thermodynamic ice-ocean coupling, we characterize the strength of eddy heat exchange, and subsequent sea-ice melting, that occurs at the edge of an area of sea ice using parameters accessible to coarser continuum climate models.

XX need something here ?XX

2 Methods

The Arctic is rapidly transitioning from a perennial sea ice regime to a seasonal one, where the majority of Arctic sea ice is relatively flat first-year sea ice that melts during

the summer season [*Kwok and Rothrock*, 2009; *Stroeve et al.*, 2012]. We therefore design ocean circulation model experiments that represent melting at the edge of, or near a newly opened gap in, first-year sea ice in summer, when the ice and ocean are exposed to strong shortwave radiative forcing. Model simulations use the MIT general circulation model [MITgcm, *Marshall and Hill*, 1997; *Losch et al.*, 2010], and simulate sea-ice evolution based on the two-layer thermodynamic model of *Winton* [2000]. A net heat flux from the ocean to the sea ice is applied to only change the local sea-ice thickness, until the thickness is reduced below 10 cm, at which point it only changes ice concentration (area). Vertical mixing is realized using the K-profile parameterization [*Large et al.*, 1994]. The ice-ocean heat flux computed using a typical bulk heat transfer parameterization appropriate for marginal ice zones [*McPhee*, 1992; *McPhee and Morison*, 2001]. We perform a sensitivity study in which we double or halve the ice-ocean heat transfer coefficient in the Supporting Information, XX.

There is no explicit horizontal diffusion of temperature and salinity. Horizontal eddy viscosity is represented by the Smagorinsky scheme. We use an adapted version of the *Deremble et al.* [2013] atmospheric boundary layer model to simulate the turbulent fluxes between the ocean, sea ice, and atmosphere, as discussed in *Horvat et al.* [2016]. The ice is free to moves, though there is no applied wind stress in our prescribed forcing fields and the initial ocean currents set to zero. Dynamical ice effects are therefore weak compared to the thermodynamic ones explored below, which allows us to explore a purely thermodynamically-driven regime.

The model domain is a rectangular, zonally re-entrant channel, 60 km by 30 km by 1000 m. The horizontal grid spacing is 100 meters, with a vertical grid spacing of 1 m over the top 50 meters, increasing by 20% at each subsequent grid point. The ocean is initialized using July climatological temperature and salinity profiles from the Fram Strait at 80°N, 0° E [*Carton and Giese*, 2008], with the top 50 meters of the water column homogenized to create a mixed layer. Initially the northern half of the model domain is covered by sea ice with a concentration of 100%, thickness of 1 meter, and internal temperature of -5° C. The top 50 m of the initial temperature field is seeded with white noise uniformly distributed between ± 0.025°C. The atmospheric radiative forcing fields include a horizontally and temporally uniform (no diurnal cycle) shortwave forcing of 320 W/m^2 and a longwave forcing of 240 W/m^2, drawn from May-July climatological averages at 80°N, 0°E. The specified forcing leads to a net heating of roughly 100 W/m^2 in the open

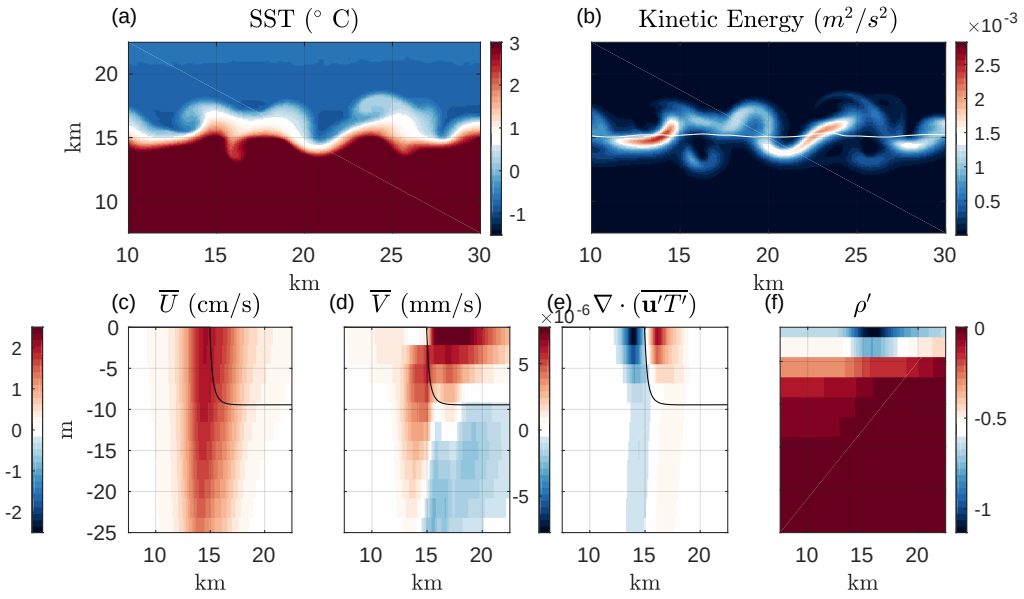

Figure 1. Ocean circulation in the ice-edge experiment (a-f) Fields at day 14 of the simulation. (a) Top 10-meter average ocean temperature. (b) Top 10 meter average ocean kinetic energy. White line denotes the position of the ice edge. (c) Zonal average along-ice-edge velocity field $\overline{u}$ in units of cm/s (d) zonal average cross-ice-edge velocity field $\overline{v}$ in units of mm/s. Plots (c-d) share a single color bar. Black line in (c-d) is zonally-averaged sea-ice thickness curve, multiplied by -10, at day 14. (e) Magnitude of eddy buoyancy XX $\overline{v'b'} + \overline{w'b'}$. Colors show negative values and contours show positive values. (f) Zonal mean density anomaly. Colorbar spacing is O(1 kg/m^3). Contour spacing is O(0.01 kg/m^3), emphasizing the sub-surface density field.

water and a net heating of 10 W/m^2 of the ice. We examine the sensitivity of the results that follow to the initial stratification, applied forcing, and ocean-ice exchange in the Supporting Information (Sec. S1-S3, Fig.s S1-S3).

3 Results

Figs. 1(a-f) show the ocean circulation that develops at the ice edge by model day 14. The prescribed heat fluxes warm the ice-free region, and also lead to sea-ice melting (Fig. 1a). Under-ice regions are then cooler and fresher than ice-free regions, and a buoyancy gradient develops at the surface near the ice edge (Fig. 1f)that is dominated by the cross-edge salinity gradient. As the sea ice melts, the under-ice freshwater forcing strengthens the vertical ocean stratification. Before an ocean circulation and mixing can develop, this surface lens of fresher water is confined to just below the sea-ice base.

The cross-ice edge buoyancy gradient is balanced by an along-ice-edge jet with magnitude $\overline{u}^x$, where $\overline{(\cdot)}^x$ indicates a zonal mean along the ice edge (Fig. 1c, units of cm/s). A comparatively weak ageostrophic secondary circulation of magnitude $\overline{v}^x$ develops perpendicular to the along-ice-edge jet (Fig. 1d, units of mm/s). As the ocean circulation grows, vertical motions associated with the ageostrophic circulation and eddies mix the fresh top ocean model layer with the saltier water below, deepening the penetration of fresh water near the ice edge. Were the sea ice in motion, stress at the ice-ocean interface would lead to a shear in the under-ice velocity profile, and then to vertical mixing that could deepen the freshwater lens, though this effect is weak in these experiments.

As the effect of temperature on density is small compared to that of salinity, the ageostrophic circulation flows down the salinity-induced pressure gradient (up the temperature gradient) across the ice edge, transporting relatively warm open-ocean surface water to under the ice and leading to further melting (Fig. 1a,f). This melting near the ice edge increases the local salinity gradient, strengthening the jet, which becomes unstable. Eddies grow rapidly at the ice edge (Fig. 1b), exchange salinity laterally and vertically, with strong positive eddy heat fluxes near the surface under the ice (Fig. 1e, warm colors).

3.1 The effect of ocean circulation on sea-ice melting

The time evolution of the zonal-mean ocean buoyancy is,

$$\frac{\partial \overline{b}^x}{\partial t} + \overline{\mathbf{u}}^x \cdot \nabla \overline{b}^x = \overline{S}^x[b] - \nabla \cdot (\overline{u'b'}^x, \overline{v'b'}^x, \overline{w'b'}^x) = \overline{S}^x[b] - \nabla \cdot \mathbf{F}[b], \tag{1}$$

where primed quantities are anomalies from the zonal mean, $\mathbf{u} = (u, v, w)$ is the ocean velocity field, b the buoyancy, $S[b]$ is the surface source of buoyancy including heat fluxes and sea-ice melting, and we denote $\mathbf{F}[C]$ as the zonal mean flux of the tracer C by the eddy field.

Sources of heat that lead to sea-ice melting include surface heating from the atmosphere and heat transport due to the ocean circulation. To separate the two we compare the above results to a similar experiment without an active ocean, in the sense that ocean velocities are set to zero. Given that horizontal diffusion is also zero, only (weak) vertical diffusion occurs in the ocean in this case. Because of the horizontally homogeneous imposed forcing fields, with the ocean inactive, sea ice in each ice-covered grid cell evolves in the same way. Sea-ice volume melt rates are significantly higher with the ocean model active (Fig. 2c, blue solid line) compared to when the ocean model is inactive (Fig. 2c,

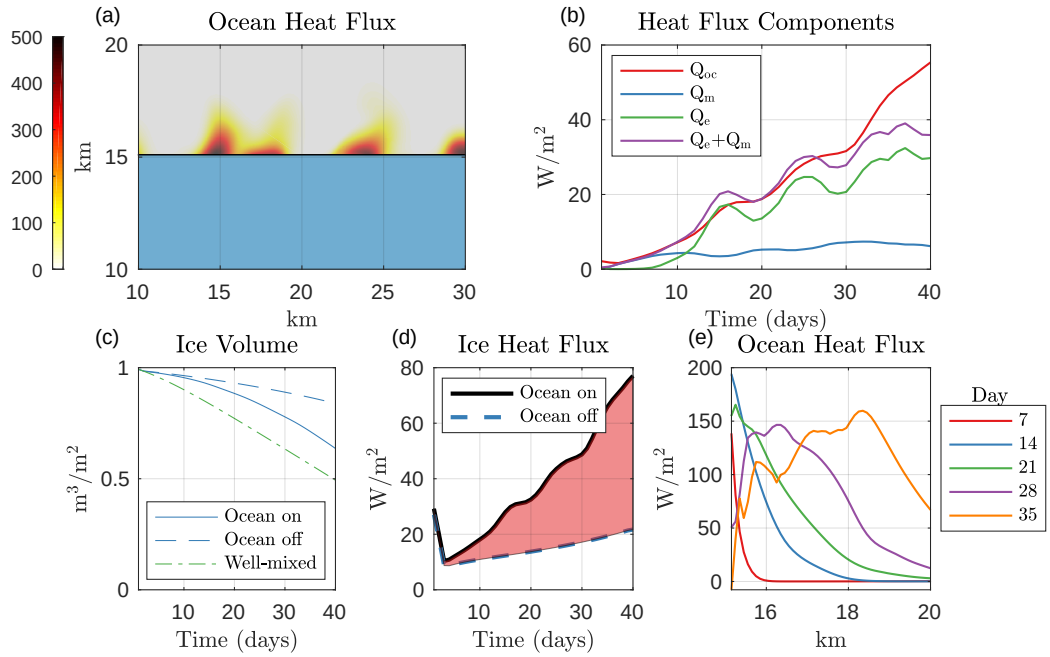

153 **Figure 2. Sea-ice melting and heat fluxes.** (a) Heat flux due to ocean circulation, $Q_{\rm oc}(\mathbf{x},t)$, (W/m^2) at
154 model day 14. (b) Domain-averaged heat fluxes from ocean circulation (red line), the zonal-mean circula-
155 tion (blue line), the effect of ocean eddies (green line), and the sum of the mean and eddy fluxes (purple).
156 (c) Curves of average sea-ice volume as a function of time for (solid) the simulation with active ocean, and
157 (dashed) a simulation with the ocean model inactive. (d) Latent heat fluxes derived from sea-ice volume
158 evolution. Red shaded area is the average ocean circulation heat flux $\overline{Q}_{\rm oc}$. (e) Zonal-mean ocean heat flux
159 $\overline{Q}^x_{\rm oc}(y,t)$ as a function of meridional distance into the ice at selected model days, with $y = 0$ corresponding to
160 the initial ice edge.

blue dashed line), indicating the critical role of heat transport by ocean eddies in leading to floe melting. In modern climate models, any heat flux to the upper ocean is mixed horizontally over a single model timestep. In Fig. 2c (green line), we plot the evolution of sea ice volume, if the ocean surface heating were evenly applied throughout the domain. A large fraction of this heat flux is sequestered away from the ice, in the case of rapid horizontal mixing case sea ice volume declines significantly more rapidly.

XXX FIX ALL NUMBERS IN THIS SECTION XXX

For both simulations, we compute a latent heat flux field, $Q(\mathbf{x},t)$, implied by sea-ice volume changes,

$$Q(\mathbf{x},t) = L_f \rho_i \frac{\partial V(\mathbf{x},t)}{\partial t}, \tag{2}$$

where $V(\mathbf{x},t)$ is the sea-ice volume field. We compute the heat flux due to ocean circulation, $Q_{\mathrm{oc}}(\mathbf{x})$, as the difference between the results of the runs with ocean dynamics on and off,

$$Q_{\mathrm{oc}}(\mathbf{x},t) = Q_{\mathrm{on}}(\mathbf{x},t) - Q_{\mathrm{off}}(\mathbf{x},t). \tag{3}$$

We plot the spatial average of each latent heat flux field, $\overline{Q}^{xy}_{\mathrm{on}}(t)$ (Fig. 2d, black line), $\overline{Q}^{xy}_{\mathrm{off}}(t)$ (Fig. 2d, blue line), and $\overline{Q}^{xy}_{\mathrm{oc}}(t)$ (Fig. 2d, red shaded region), where $\overline{(\cdot)}^{xy}$ denotes a horizontal average. $\overline{Q}^{xy}_{\mathrm{oc}}$ grows to 20 W/m^2 after 21 days, significantly larger than the "ocean off" heat flux of 14 W/m^2 at the same time. By day 40, $\overline{Q}^{xy}_{\mathrm{oc}}$ is 55 W/m^2 compared to $\overline{Q}^{xy}_{\mathrm{off}}$ = 21 W/m^2. Fig. 2a shows $Q_{\mathrm{oc}}(\mathbf{x},t)$ at day 14, with the along-ice-edge mean $\overline{Q}^{x}_{\mathrm{oc}}(y,t)$ plotted in Fig. 2e every seven days.

Local values of $Q_{\mathrm{oc}}(\mathbf{x},t)$ can exceed several hundred W/m^2 when the eddies and mean flow are actively transporting warm water toward underneath the ice (warm colors, Fig. 2a). This again demonstrates the critical role of ocean dynamics due to eddy mixing in melting floes near the edges, a process not represented in current climate models, and therefore requiring a parameterization. Far from the ice edge, where the ocean circulation does not reach, $Q_{\mathrm{oc}}(\mathbf{x},t) \approx 0$.

3.2 The effect of eddies on sea-ice melting

We integrate the zonally averaged temperature equation in ice-covered regions over a depth H, and multiply by the ocean specific heat capacity, c_p, and by the ocean density,

ρ, leading to the zonal-mean heat budget of this surface layer,

$$\begin{aligned} & c_p \rho_0 \int_{-H}^{0} dz \frac{\partial \overline{T}^x}{\partial t} \\ &= Q_\mathrm{s} - L_f \rho_i \frac{\partial \overline{V}^x}{\partial t} - c_p \rho_0 \int_{-H}^{0} dz \left(\overline{\mathbf{u}}^x \cdot \nabla \overline{T}^x - \nabla \cdot \mathbf{F} \right) \\ &= Q_\mathrm{s} - L_f \rho_i \frac{\partial \overline{V}^x}{\partial t} + Q_\mathrm{m} + Q_\mathrm{e}, \end{aligned}$$

where Q_s is the net surface heating by air-sea fluxes, Q_mean is the heating arising from zonal mean ocean flows, and Q_e is the eddy heat flux. Under the sea ice, we assume the ocean temperature is approximately at freezing, and therefore $\partial \overline{T}^x / \partial t \equiv 0$, such that the left-hand side of the above equation vanishes. Averaging each term over the entire ice-covered domain, we obtain an equation for the evolution of sea-ice volume,

$$L_f \rho_i \frac{\partial V}{\partial t} = Q_\mathrm{on/off} = Q_\mathrm{m} + Q_\mathrm{e} + Q_\mathrm{s}. \tag{4}$$

With the ocean circulation off, $Q_\mathrm{m} = Q_\mathrm{e} = 0$, and,

$$\begin{aligned} Q_\mathrm{oc} \equiv Q_\mathrm{on} - Q_\mathrm{off} &= Q_\mathrm{m} + Q_\mathrm{e} \\ &\approx Q_\mathrm{m} + Q_\mathrm{e}. \end{aligned} \tag{5}$$

In general, the under-ice temperature is slightly above freezing as the heat transported to under the ice floe is not instantaneously absorbed by the ice base, though approximating the temperature to be at freezing under the ice is appropriate throughout the experimental period shown in Fig. 2.

Fig. 2b plots the terms in (5), the area-averaged contributions to the total sea-ice melting due to ocean dynamics, Q_oc (also shown by the shaded region in Fig. 2d). The melting heat flux due to the mean ocean currents grows and saturates at about 4 W/m^2 by day 7. The heat flux due to eddies grows rapidly, surpassing Q_m by day 12, increasing by roughly 2 W/m^2 per day until day 40. Over this period, the sum of ocean heat fluxes computed via Eq. 5 (Fig. 2b, purple line) tracks Q_oc, justifying our previous assumptions. Over time, as the sea-ice edge begins to depart from zonal symmetry, the approximations used to derive Eq. (5) are no longer valid.

3.3 Parameterizing sea-ice melting due to ocean eddies

In current climate models, sub-grid-scale sea-ice floes and ocean eddies are not resolved, and heat absorbed by an open ocean area is assumed immediately distributed un-

der the ice within the same grid box, leading to known biases [*Holland*, 2003]. Because the effect of eddies leads to a significant difference in ice evolution both from this well-mixed assumption and the assumption of no ocean variability (see Fig. 2c) we wish to correctly represent the eddy heat transport between ice-covered and ice-free regions, and the resulting contribution to ice melting, Q_{oc} (Eq. 5). We therefore seek a simple parameterization of the eddy heat exchange that we showed above to control sea-ice melting.

Consider the heat budget of two regions: one corresponding to the top H meters of the ice-free region and the other to the top H meters of the ice-covered region. The ice-free regions are characterized by a freely varying temperature, T_o, and salinity, S_o, and the under-ice regions have a variable salinity, S_i, with temperature fixed at the ocean freezing point, T_f.

While the secondary circulation develops faster than the eddies, its effect on melting is significantly smaller than that of eddies once they reach finite amplitude. We estimate Q_{e} according to the following scaling,

$$Q_{\mathrm{e}} \approx c_p \rho V \frac{\Delta T}{\Delta X}, \tag{6}$$

with units of W/m^2. The factor $\Delta T = T_o - T_f$ is the temperature difference between the ice-free and ice-covered regions, ΔX is the eddy length scale, and the velocity V represents the strength of the eddy exchange. The length scale ΔX is calculated as the decorrelation length scale of the meridional velocity field, the first zero of the correlation function $C(y,\xi) = \overline{v(x,y)v(x+\xi,y)}^{x}$. The time evolution of ΔX is shown in Fig. 3a, and based on this as well as for simplicity, we fix $\Delta X = 5$ km in all cases, assuming the effect of eddies are felt roughly 2.5 km into the ice edge.

We now develop a sequence of approximations for the eddy heat flux contribution to the sea-ice melting, Q_{e}, culminating with a version that can serve as the base for a parameterization in future climate models. We begin by approximating the contribution of ocean eddies to melting using the full model simulation output. The solid line in Fig. 3b shows ΔT^0, computed as the difference in temperature between the ice-covered and ice-free regions over a depth $H = 5$ m. To estimate the eddy velocity, we use a quasigeostrophic scaling [*Andrews and McIntyre*, 1978], for the eddy-induced overturning velocity,

$$v \approx \frac{\partial}{\partial z}\left(\overline{v'b'}/\bar{b}_z\right). \tag{7}$$

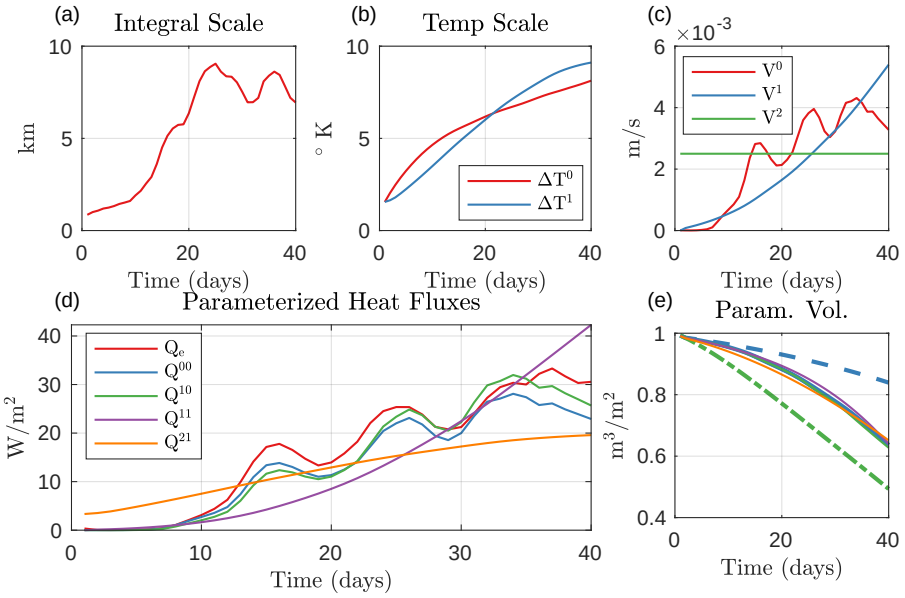

Figure 3. Components of, and parameterization of, the eddy heat flux Q_e. (a) The eddy length scale ΔX computed from model results. (b) The two-box temperature difference between ice and ice-free regions, computed from the modeled ocean temperature fields (black line) or computed from balancing the ocean surface warming with latent heat from sea-ice melting (dashed line). (c) Velocity scaling estimates for the cross-ice velocity V using the quasigeostrophic scaling of *Andrews and McIntyre* [1978], either computed directly (black line), based on the scaling of *Haine and Marshall* [1998] (green line), or a constant estimate (red line) (d)Estimates of the eddy heat flux compared to its actual value (black solid line). Definitions of each estimate of Q_e are tabulated in Table 1. Using computed values of ΔT and V ($Q^{(0,0)}$, dashed black line), an estimate of ΔT with V computed from model results ($Q^{(1,0)}$, solid red line), an estimate of ΔT with parameterized V from *Haine and Marshall* [1998] ($Q^{(1,1)}$, dashed red line), or an estimate of ΔT with a fixed V ($Q^{(1,2)}$, green line) (e) Same as Fig. **??**, now including volume curves obtained by integrating Eq. **??** with $Q_m = 4\text{W/m}^2$ and Q_e defined by the parameterizations in (d).

Name	Estimate of Δ T	Estimate of V
Q_{eddy}	— Computed via Eq. 5 —	
$Q_{eddy}^{(0,0)}$	From Simulation	From Simulation (Eq. 7)
$Q_{eddy}^{(1,0)}$	Eq. 8	From Simulation (Eq. 7)
$Q_{eddy}^{(1,1)}$	Eq. 8	Eq. (12)
$Q_{eddy}^{(1,2)}$	Eq. 8	Constant

Table 1. Definitions of the ocean eddy heat flux Q_e and parameterizations detailed in the text. Estimates of T and V form the components of Eq. 6. The superscript indices on Q refer to the level of approximation used for the cross ice-edge temperature difference and for the velocity scale, correspondingly.

The first estimate of the eddy velocity scale, V^0, is computed as the average of v over a depth H at the ice edge (Fig. 3c, black line).

The first estimate for the eddy-induced melting heat flux, computed directly from the simulation output fields, is denoted $Q_e^{(0,0)}$ (Fig. 3d, blue line), and completes Eq. 6 using V^0 and T^0. A list of all notation and variants of the parameterizations presented is given in Table 1). The approximation $Q_e^{(0,0)}$ is well-correlated with the eddy contribution to the melting heat flux, Q_e (Fig. 3d, solid black line) over the first 40 days, with a detrended correlation coefficient $r^2 = .85$ between the two time series, which in addition to the visual confirmation of Fig. 3d gives confidence that the downgradient approximation of Eq. 6 can estimate the melting rate of sea ice in this context.

Climate models may not resolve the required horizontal variation in temperature or circulation, and therefore we seek alternative representations of V and T based on properties of the large-scale forcing. The time rate of change of the ice-free surface temperature is a function of the surface heat flux over open water, Q_s, with units W/m^2 of open water. The average of this flux over the entire model domain (or over a grid cell of a global climate model) is equal to ϕQ_s, where ϕ is the open water fraction. Neglecting vertical mixing of heat, the remaining sink of surface heat is latent heat used to melt sea ice after being transported across the ice edge (the ice-covered surface ocean region is assumed to stay at its freezing point). We approximate,

$$H c_p \rho \phi \frac{\partial T_o}{\partial t} \approx Q_s \phi - Q_e, \tag{8}$$

We choose $H = 5$ meters based on the resolved density profile of the ice-free ocean (i.e., Fig. **??**), which evolves as a function of depth due to the exponential penetration of shortwave radiation and the growing ocean circulation (XX - should I add something to the SI). As the left-hand-side of Eq. 8 represents the heat content available to melt sea ice, choosing a larger value of H incorporates sub-surface waters separated from the surface warming and ice base that do not lead to melting. In that case, the parameterization under-estimates ΔT and subsequently Q_e (SI, Fig. XX).

Fig. 3b shows the parameterized $\Delta T^1 = T_o - T_f$ (blue line) calculated using (8). This approximation underestimates the warming of the surface layer initially, and overestimates it at later times, but is adequate overall. An estimate of the eddy heat flux using ΔT^1 and V^0, $Q_\mathrm{e}^{1,0}$, (Fig. 3d, green line) is well-correlated with the computed eddy heat flux Q_e over this period.

Next, we scale the magnitude of the meridional eddy flux in Eq. 9 according to *Haine and Marshall* [1998], with $\overline{v'b'}^x \approx -C_1 \bar{b}_z H^2 \bar{b}_y^x / f$, where C_1 is a non-dimensional "efficiency parameter",

$$v \sim \frac{\partial}{\partial z}\left(\frac{\overline{v'b'}^x}{\bar{b}_z^x}\right) \approx \frac{1}{H}\left(\frac{\overline{v'b'}^x}{\bar{b}_z^x}\right) \approx -C_1 \frac{H}{f}\bar{b}_y^x \approx C_1 \frac{-H}{f}\frac{\Delta B}{\Delta X} \tag{9}$$

We approximate the change in buoyancy resulting from salinity variations alone using a linear equation of state, $\rho = \rho_0(1 + \beta(S - S_0))$. We express the buoyancy difference between ice-free and ice-covered regions as,

$$\Delta B = -g\beta\Delta S, \tag{10}$$

where $\beta \approx 8 \cdot 10^{-4}$ psu^{-1}. The time rate of change of the salt content of the upper layer of the under-ice regions is equal to $c\rho_0 H \partial S_i/\partial t$, where $c = 1 - \phi$ is the sea-ice concentration and S_i is the under-ice salinity. Assuming the sea ice to be fresh, the freshwater flux due to melting sea ice is $\rho_i \partial V_i/\partial t$ kg/m^2/s, and therefore the time rate of change of the under-ice salinity is expressed in terms of the melting of sea ice,

$$\frac{\partial S_i}{\partial t} = -\frac{S_i}{H}\frac{\rho_i}{\rho_0}\frac{\partial V_i}{\partial t}\frac{1}{c}. \tag{11}$$

We now estimate the eddy velocity scale by integrating the under-ice salinity equation, finding,

$$V^1 = C_1 \frac{g\beta}{f\Delta X}\frac{\rho_i}{\rho_0}\int S_i \frac{\partial V_i}{\partial t}\frac{1}{c}dt. \tag{12}$$

Importantly, all quantities in equation (12) can be computed in a coarse climate model. We find $C_1 \approx 0.1$ gives the best fit to Q_e, and plot V^1 as a blue line in Fig. 3. The es-

timate $Q_e^{1,1}$ is computed from ΔT^1 and V^1 (Fig. 3d purple line) and, even with the broad simplification of Eq. 12, represents the general trend in Q_e. This parameterization may be evaluated in a climate model, by integrating forward equations starting from the time at which the net heat flux is generally warming, and sea ice begins to melt. In practice, to correctly estimate the mixing of ice-free and ice-covered regions would require tracking the ice-free surface temperature, under-ice surface temperature, and under-ice salinity separately (using a scheme like that designed by *Holland* [2003] or *Roach et al.* [2018]).

We compute an even simpler estimate for the contribution of sub-grid scale ocean eddies to sea ice, fixing the cross-ice velocity scale $V^2 = 2$ mm/s (green line, Fig. 3c) and thereby dropping the need to track under-ice salinity. The resulting estimate for the eddy heat flux, $Q_e^{(1,2)}$ (gold line, Fig. 3d) represents the trend in Q_e but over-estimates the rate of sea-ice melting when the eddies are inactive. Despite the gross simplification, each of these parameterization may be adequate to describe the transfer of heat from ocean to ice. Fig. 3e superimposes on top of Fig. 2c curves of sea ice volume obtained by integrating forward equation **??** using $Q_m \equiv 4\text{W/m}^2$ and for each of the parameteriations of Q_e plotted in Fig. 3d. Despite the simplifications involved in calculating both the mean and eddy heat fluxes, each volume curve approximates the resolved sea ice volume curve.

In the Supporting Information (Text S1-S3, Fig.s S1-S3), we reproduce Fig. 3d-e, varying the applied external forcing by an amount $\Delta Q \pm 50\text{W/m}^2$, extending the stratification from 50 meters to the surface, and increase or decreasing the ice-ocean heat transfer coefficient by a factor of ± 2. Generally, the parameterization is robust to these wide changes. It breaks down at the extreme high range of external forcing (above $\Delta Q = 30$ W/m^2): in this case surface melting dominates sea ice volume change. When we extend the near-surface stratification to the top 10 meters, the instability is suppressed, and $Q_e \approx 0$. (XX WILL UPDATES WHEN ALL RUNS DONE XX).

4 Discussion and Conclusions

Using simulations of an ocean near a sea-ice edge in a domain corresponding to a single climate model grid cell, we showed that ocean eddies that cannot be resolved by typical state-of-the-art climate models can drive sea-ice melting. The eddies transport heat from the open ocean toward the ice, strongly enhancing melting near the ice edge. We then developed and examined a scaling argument describing the effects on melting due

to eddies generated at the edge of a floe that can be used in future climate models to replace non-physical horizontal mixing schemes that do not partition ocean heating between ice-covered and ice-free regions. The scaling derived here reproduces the modeled sea-ice volume evolution over a period of 40 days, corresponding to a significant portion of the sea-ice melting season, and is a function of model state variables that are resolved by coarse-grid sea ice and climate models.

The study of emergent sub-grid scale sea-ice state variables such as the floe size distribution and their effect on large-scale climate is growing rapidly [e.g., *Horvat and Tziperman*, 2015; *Zhang et al.*, 2016; *Horvat and Tziperman*, 2017; *Bennetts et al.*, 2017; *Roach et al.*, 2018]. More work is needed to investigate how the results obtained here can be applied to generalized floe geometry, and to constrain the relative strength of the effect of eddies versus other processes that mix heat in the upper ocean, including wind, waves, and sea-ice motion. The work presented here can be used to improve upon the implicit instantaneous numerical "mixing" of heat between open ocean and sea ice, though this will require a full assessment of the mixing processes that transfer heat in the upper ice-covered oceans.

The scenario examined above does not include sea ice forced by large-scale wind or ocean currents, though drift speeds of sea ice floes can be up to 10 kilometers per day **?**. Instability growth rates examined here are O(1/day), and eddy scales of O(2 km), suggesting the analysis presented above is appropriate only in situations where ice drift speeds are O(1 km/day) and lower. To modify the parameterization above for such dynamical scenarios would likely require experiments with moving, thermodynamically active sea ice floes that resolve both the sharp gradients in surface forcing at the edge of floes but also their drift forced by wind and ocean current. The instability investigated here competes with and is modified by other effects, and represents but one of several mixing processes that can influence the sea ice. For example, stresses from ice or ocean motions can lead to shear that will enhance vertical mixing and energize an Ekman overturning circulation, both of which will deepen the freshwater lens that forms under the melting ice and may lead to other dynamical instabilities [*Hakkinen*, 1986; *Manucharyan and Thompson*, 2017].

Describing the rich interactions between eddies and ice melting, including the many processes merely briefly discussed above, remains an open and important problem, yet there have to date been no observational investigations of the melting of a single floe nor

the developing ocean circulation at the floe edge. Field observations will be an important part of constraining these processes, and together with floe-scale process modeling as will lead to a better representation of the effects of small-scale ice-ocean interactions on high-latitude climate.

Acknowledgments

The authors would like to thank Andy Hogg and two anonymous reviewers for their most constructive comments. Files required to reproduce experiments shown here are publicly available at `https://www.seas.harvard.edu/climate/eli/Downloads`. This work was funded by NSF Physical Oceanography program, grant OCE-1535800 and by the NASA ROSES program, grant number NNX14AH39G. CH was supported by the NOAA Climate and Global Change Postdoctoral Fellowship Program, administered by UCAR's Cooperative Programs for the Advancement of Earth System Science (CPAESS), sponsored in part through cooperative agreement number NA16NWS4620043, Years 2017–2021, with the National Oceanic and Atmospheric Administration (NOAA), U.S. Department of Commerce (DOC). The views expressed in this paper are those of the author(s) and do not necessarily reflect the view of DOC, any of its sub-agencies, or any other Sponsors of CPAESS and/or UCAR. ET thanks the Weizmann institute for its hospitality during parts of this work. CH thanks the National Institute of Water and Atmospheric Science as well as the Frenchboro Trust for their hospitality during parts of this work.

References

Andrews, D. G., and M. E. McIntyre (1978), Generalized Eliassen-Palm and Charney-Drazin Theorems for Waves oin Axismmetric Mean Flows in Compressible Atmospheres, *J. Atmos. Sci.*, *35*(2), 175–185, doi:10.1175/1520-0469(1978)035<0175:GEPACD>2.0.CO;2.

Årthun, M., P. R. Holland, K. W. Nicholls, and D. L. Feltham (2013), Eddy-Driven Exchange between the Open Ocean and a Sub–Ice Shelf Cavity, *J. Phys. Ocean.*, *43*(11), 2372–2387, doi:10.1175/JPO-D-13-0137.1.

Bennetts, L. G., S. O'Farrell, and P. Uotila (2017), Brief communication: Impacts of ocean-wave-induced breakup of Antarctic sea ice via thermodynamics in a stand-alone version of the CICE sea-ice model, *Cryosphere*, *11*(3), 1035–1040, doi:10.5194/tc-11-1035-2017.

Carton, J. A., and B. S. Giese (2008), A Reanalysis of Ocean Climate Using Simple Ocean Data Assimilation (SODA), *Mon. Weath. Rev.*, *136*(8), 2999–3017, doi:10.1175/2007MWR1978.1.

Deremble, B., N. Wienders, and W. K. Dewar (2013), CheapAML: A Simple, Atmospheric Boundary Layer Model for Use in Ocean-Only Model Calculations, *Mon. Weath. Rev.*, *141*(2), 809–821, doi:10.1175/MWR-D-11-00254.1.

Haine, T. W. N., and J. Marshall (1998), Gravitational, Symmetric, and Baroclinic Instability of the Ocean Mixed Layer, *J. Phys. Ocean.*, *28*(4), 634–658, doi:10.1175/1520-0485(1998)028<0634:GSABIO>2.0.CO;2.

Hakkinen, S. (1986), Coupled ice-ocean dynamics in the marginal ice zones: Upwelling/downwelling and eddy generation, *J. Geophys. Res.*, *91*(C1), 819–832, doi:10.1029/JC091iC01p00819.

Holland, M. M. (2003), An improved single-column model representation of ocean mixing associated with summertime leads: Results from a SHEBA case study, *J. Geophys. Res.*, *108*(C4), 1–10, doi:10.1029/2002JC001557.

Horvat, C., and E. Tziperman (2015), A prognostic model of the sea-ice floe size and thickness distribution, *Cryosphere*, *9*(6), 2119–2134, doi:10.5194/tc-9-2119-2015.

Horvat, C., and E. Tziperman (2017), The evolution of scaling laws in the sea ice floe size distribution, *J. Geophys. Res. Ocean.*, *122*(9), 7630–7650, doi:10.1002/2016JC012573.

Horvat, C., E. Tziperman, and J. M. Campin (2016), Interaction of sea ice floe size, ocean eddies, and sea ice melting, *Geophys. Res. Lett.*, *43*(15), 8083–8090, doi:10.1002/2016GL069742.

Kwok, R., and D. a. Rothrock (2009), Decline in Arctic sea ice thickness from submarine and ICESat records: 1958-2008, *Geophys. Res. Lett.*, *36*(15), doi:10.1029/2009GL039035.

Large, W. G., J. C. McWilliams, and S. C. Doney (1994), Oceanic vertical mixing: A review and a model with a nonlocal boundary layer parameterization, *Rev. Geophys.*, *32*(4), 363, doi:10.1029/94RG01872.

Lei, R., N. Li, P. Heil, B. Cheng, Z. Zhang, and B. Sun (2014), Multiyear sea ice thermal regimes and oceanic heat flux derived from an ice mass balance buoy in the Arctic Ocean, *J. Geophys. Res.*, *119*(1), 537–547, doi:10.1002/2012JC008731.

Losch, M., D. Menemenlis, J. M. Campin, P. Heimbach, and C. Hill (2010), On the formulation of sea-ice models. Part 1: Effects of different solver implementations and pa-

rameterizations, *Ocean Model.*, *33*(1-2), 129–144, doi:10.1016/j.ocemod.2009.12.008.

Manucharyan, G. E., and A. F. Thompson (2017), Submesoscale Sea Ice-Ocean Interactions in Marginal Ice Zones, *J. Geophys. Res. Ocean.*, *122*(12), 9455–9475, doi:10.1002/2017JC012895.

Markus, T., J. C. Stroeve, and J. Miller (2009), Recent changes in Arctic sea ice melt onset, freezeup, and melt season length, *J. Geophys. Res.*, *114*(C12), C12,024, doi:10.1029/2009JC005436.

Marshall, J., and C. Hill (1997), Hydrostatic, quasi-hydrostatic, and nonhydrostatic ocean modeling, *J. Geophys. Res. Ocean.*, *102*, 5733–5752.

Maslanik, J., J. Stroeve, C. Fowler, and W. Emery (2011), Distribution and trends in Arctic sea ice age through spring 2011, *Geophys. Res. Lett.*, *38*(13), 2–7, doi:10.1029/2011GL047735.

Matsumura, Y., and H. Hasumi (2008), Brine-driven eddies under sea ice leads and their impact on the Arctic Ocean mixed layer, *J. Phys. Ocean.*, *38*(1), 146–163, doi:10.1175/2007JPO3620.1.

McPhee, M., and J. Morison (2001), Under-ice Boundary Layer, in *Encycl. Ocean Sci.*, pp. 3071–3078, Elsevier, doi:10.1006/rwos.2001.0146.

McPhee, M. G. (1992), Turbulent heat flux in the upper ocean under sea ice, *J. Geophys. Res.*, *97*(C4), 5365, doi:10.1029/92JC00239.

Peralta-Ferriz, C., and R. A. Woodgate (2015), Seasonal and interannual variability of pan-Arctic surface mixed layer properties from 1979 to 2012 from hydrographic data, and the dominance of stratification for multiyear mixed layer depth shoaling, *Prog. Ocean.*, *134*, 19–53, doi:10.1016/j.pocean.2014.12.005.

Perovich, D., J. Richter-Menge, C. Polashenski, B. Elder, T. Arbetter, and O. Brennick (2014), Sea ice mass balance observations from the North Pole Environmental Observatory, *Geophys. Res. Lett.*, *41*(6), 2019–2025, doi:10.1002/2014GL059356.

Perovich, D. K. (2003), Thin and thinner: Sea ice mass balance measurements during SHEBA, *J. Geophys. Res.*, *108*(C3), 8050, doi:10.1029/2001JC001079.

Roach, L. A., S. M. Dean, C. Horvat, and C. M. Bitz (2018), Implementation of the joint sea ice floe size and thickness distribution in a global coupled ocean — sea ice model.

Screen, J. A., and I. Simmonds (2010), The central role of diminishing sea ice in recent Arctic temperature amplification, *Nature*, *464*(7293), 1334–1337, doi:10.1038/nature09051.

Steele, M. (1992), Sea ice melting and floe geometry in a simple ice-ocean model, *J. Geophys. Res. Ocean.*, *97*(C), 17,729, doi:10.1029/92JC01755.

Stroeve, J. C., M. C. Serreze, M. M. Holland, J. E. Kay, J. Malanik, and A. P. Barrett (2012), The Arctic's rapidly shrinking sea ice cover: a research synthesis, *Clim. Chang.*, *110*(3-4), 1005–1027, doi:10.1007/s10584-011-0101-1.

Winton, M. (2000), A reformulated three-layer sea ice model, *J. Atmos. Ocean. Tech.*, *17*(4), 525–531, doi:10.1175/1520-0426(2000)017<0525:ARTLSI>2.0.CO;2.

Zhang, J., H. Stern, B. Hwang, A. Schweiger, M. Steele, M. Stark, and H. C. Graber (2016), Modeling the seasonal evolution of the Arctic sea ice floe size distribution, *Elem. Sci. Anthr.*, *4*(1), 000,126, doi:10.12952/journal.elementa.000126.